International Journal of Biological Macromolecules xxx (2017) xxx–xxx

Contents lists available at ScienceDirect

International Journal of Biological Macromolecules

journal homepage: www.elsevier.com/locate/ijbiomac

Non-covalent DNA binding, protein interaction, DNA cleavage and cytotoxicity of [Cu(quamol)Cl]·H_2O

Somasundaram Sangeetha, Mariappan Murali*

Coordination and Bioinorganic Chemistry Research Laboratory, Department of Chemistry, National College (Autonomous), Tiruchirappalli 620 001, India

ARTICLE INFO

Article history:
Received 13 June 2017
Received in revised form 10 October 2017
Accepted 20 October 2017
Available online xxx

Keywords:
Copper(II) complex
Partial intercalation
Binding constant
Static quenching
Oxidative cleavage
Cytotoxicity

ABSTRACT

A copper(II) complex [Cu^{II}(quamol)Cl]·H_2O, where H(quamol) is *N*-2-(quinolylmethylidene)aminophenol, has been isolated. The solution structure of the complex has been assessed to be distorted square-planar. The complex displays a ligand field band in the visible region (608 nm) and also show axial EPR spectrum in DMF at 77 K with $g_{||} > g_{\perp}$ indicating a $d_x{}^2{}_{-y}{}^2$ ground state. The $g_{||}$ and $A_{||}$ values of 2.265 and 153×10^{-4} cm^{-1}, respectively, conform to a square-based CuN_2OCl chromophore. The interaction of the complex with calf thymus (CT) DNA has been explored by using absorption ($K_b = 2.48 \times 10^5$ M^{-1}), emission ($K_{app} = 7.72 \times 10^4$ M^{-1}) and circular dichroic (CD) spectral measurements, which reveals that a complex interacts strongly with DNA through partial intercalation. The electrochemical studies indicate that Cu(II) binds to DNA more strongly than Cu(I). It cleaves ϕX174 supercoiled phage DNA in the presence of ascorbic acid as a reducing agent. Meanwhile, the interaction of the complex with bovine serum albumin (BSA) indicates that the complex can markedly quench the intrinsic fluorescence of BSA *via* a static quenching process and cause its conformational change. Interestingly, the observed IC_{50} values for the cell lines EVSA-T (breast cancer) and M19 MEL (melanoma) are in the range of those observed with cisplatin while M19 MEL cancer cell line, complex is more active than 5-fluorouracil. The complex is non-toxic to healthy cells.

1. Introduction

Platinum(II) complexes as exemplified by cisplatin and some of its derivatives have been widely used for the treatment of various types of cancer [1]. Despite their widespread clinical use, these complexes suffer from severe toxic side effects and acquired drug resistance [2]. In an effort to improve the efficacy and overcome the side effects associated with the use of Pt-based drugs, more and more attention has been paid to investigate more effective, less toxic and target-specific metal-containing anticancer agents [3]. As a routine chemotherapeutic agent for a broad range of solid malignancies, cisplatin functions by cross-linking DNA strands through coordination of nucleic acid bases, which can subsequently induce apoptosis in cancer cells [4,5]. Thus, the mechanism of action of metal complexes in cancer cells is that they bind with the DNA of cells and inhibit the division of cancer cells [6,7]. Among three modes of non-covalently bond between metal complexes and DNA, the intercalative binding is stronger than other two binding modes (electrostatic, groove-binding) because the surface of intercalative molecule insert between the aromatic and heterocyclic base pairs [8]. Like, intercalators, groove binders also have been used extensively as antitumor, anticancer and antibacterial agents [9].

Among all metals, copper is an essential transition metal related to a wide range of aspects of life processes and especially involved in redox biology [10]. Due to its properties as a redox active metal, copper and its complexes have the ability to catalyze the generation of reactive oxygen species (ROS) that might cause the oxidative modification of cellular components such as DNA. Since Sigman's discovery of the "chemical nuclease" activity of $[Cu(phen)_2]^{2+}$ (phen = 1,10-phenanthroline) [11], copper(II) complexes containing heterocyclic bases have been extensively explored in virtue of their strong interactions with DNA *via* surface associations or intercalation [12,13] and potential DNA cleavage activities *via* hydrolytic or oxidative mechanisms [14,15]. Anticancer compounds with copper as a metal center are hypothesized to be less toxic and more potent, thus Cu(II) compounds are regarded as one of the most promising alternatives to cisplatin as anticancer substances. Nowadays, some copper(II) complexes have been reported to serve as potential anticancer and cancer inhibiting agents and several ones have been found to be active both *in vitro* and *in vivo*. Reedijk et al. have reported a novel copper(II) complex, [Cu^{II}(pyrimol)Cl], that could catalytically cleave DNA in the absence of reductant and show

* Corresponding author.
E-mail address: ma66mu@gmail.com (M. Murali).

https://doi.org/10.1016/j.ijbiomac.2017.10.131
0141-8130/

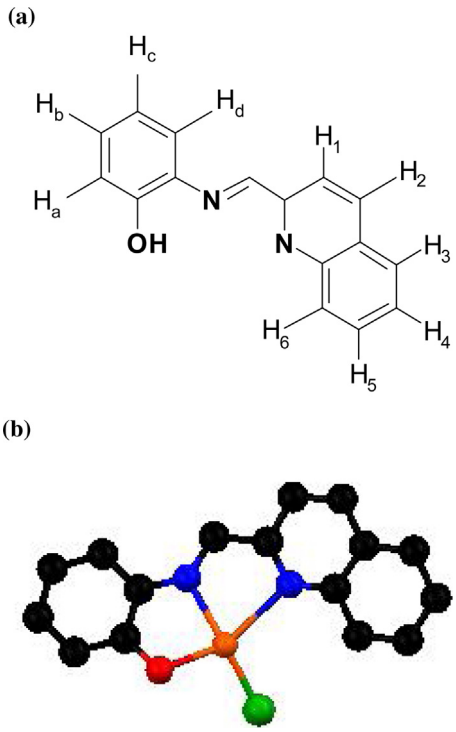

Fig. 1. (a) H(quamol) and (b) chemical structure of [Cu^{II}(quamol)Cl].

high to moderate cytotoxicity against selected cancer cell lines [16]. Ng et al. have prepared several ternary copper(II) complexes, which strongly bind to DNA and also regulate cancer cell apoptosis [17]. Palaniandavar et al. have isolated mixed ligand copper(II) complexes with diimines, which cleave DNA oxidatively and also exhibit anticancer activity [18].

When one compound can be used as drug, it can bind to carrier proteins in the blood, its solubility increases in the blood plasma and resulting in deliver to its target cells. The most important carrier protein in the blood is serum albumin [19]. Serum albumin has multiple binding sites and is able to interact with drug molecules and form a stable protein-drug complex which could affect the absorption, distribution, activity and toxicity of drugs [20]. Bovine serum albumin (BSA) is the most extensively studied serum albumin due to its structural homology with human serum albumin (HSA). It has two tryptophan residues, Trp-134 in the first domain is located within a hydrophobic binding pocket and Trp-212 in the second domain is on the surface of the molecule [21]. BSA can be used as drug carrier owing to its high conformational adaptability, biocompatibility and low cost [22].

So, in the present investigation, we have isolated redox-active copper(II) complex having the formula [Cu(quamol)Cl]·H_2O (**1**) with tridentate ligand *N*-(2-quinolylmethylidene)aminophenol, H(quamol) (Fig. 1) and have investigated its DNA binding and cleavage properties. The strength and probable mode of binding of the drugs to DNA are important for predicting the binding site of drugs at the genomic level, thereby inhibiting replication and transcription. The copper(II) complexes may interact with DNA in different modes *viz.* intercalative and groove binding [23]. External electrostatic binding has also been implicated in some cases [24]. So, it is proposed to employ electronic absorption, fluorescence emission and circular dichroic spectral studies and electrochemical techniques to diagnose the mode and extent of interaction of **1** with DNA and then to understand the DNA cleavage abilities. Affinity of **1** to BSA was investigated by UV–vis absorption, fluorescence and circular dichroism spectroscopy, which may provide important information for the transportation of the complex within the body. Further, we have studied the *in vitro* cytotoxicity of the DNA-cleaving complex towards MCF7 (breast cancer), EVSA-T (breast cancer), WIDR (colon cancer), IGROV (ovarian cancer), M19 MEL (melanoma), A498 (renal cancer) and H226 (non-small cell lung cancer) human tumor cell lines.

2. Materials and methods

Copper(II) chloride dihydrate, 2-aminophenol, 2-quinolinecarboxaldehyde, 1-methylimidazole (Aldrich), ethidium bromide (Merck) and agarose (Genei) were used as received. Adenosine-5′-monophosphate (AMP), guanosine-5′-monophosphate (GMP) and cytosine-5′-monophosphate (CMP), calf thymus (CT) DNA and superoxide dismutase were purchased from Sigma Aldrich and stored at −20 °C. The ϕX174 supercoiled phage DNA was purchased from Invitrogen Life Technologies (0.25 μg/μL) and stored at −20 °C. The bovine serum albumin (BSA) was purchased from Sigma Aldrich and stored at 4 °C. Ultrapure MilliQ water (18.2 mΩ) was used for all the experiments. The solvents were purchased from Biosolve (AR grade) and used for syntheses without further purification.

Seven human tumor cell lines MCF7 (breast cancer), EVSA-T (breast cancer), WIDR (colon cancer), IGROV (ovarian cancer), M19 MEL (melanoma), A498 (renal cancer) and H226 (non-small cell lung cancer) and a normal cell line NIH 3T3 (mouse embryonic fibroblasts) were used. Cell lines WIDR, M19 MEL, A498, IGROV and H226 belong to the currently used anti-cancer screening panel of the National Cancer Institute, USA [25]. The human breast cancer cell line MCF7 and EVSA-T are estrogen receptor $(ER)^+$/progesterone receptor $(PgR)^+$ and $(ER)^-$/$(PgR)^-$ respectively. Prior to the experiments, a mycoplasma test was carried out on all cell lines, which were found to be negative. All cell lines were maintained in a continuous logarithmic culture in RPMI (Gibco, Invitrogen, Paisley Scotland) 1640 medium with Hepes and phenol red. The medium was supplemented with 10% fetal calf serum (Gibco, Invitrogen, Paisley Scotland), pencillin 100 units/mL (Sigma, St. Louis MO, USA) and streptomycin 100 μg/mL (Sigma, St. Louis MO, USA). The cells were mildly trypsinized for passage and for use in the experiments.

2.1. Physical measurements

The elemental analyses (C, H, N) were, carried out using a Perkin-Elmer 2400 series II analyzer. The electrical conductivity was obtained with a Systronic 305 conductivity bridge, using 1×10^{-3} M solution of complex in 10% aqueous dimethylformamide (DMF). Mass spectrometry experiments were performed on a Finnigan MAT TSQ-700 equipped with a custom-made electrospray interface (ESI). Spectra were collected by constant fusion of the analyte dissolved in DMF. FTIR spectra were recorded using a Perkin-Elmer Paragon 1000 FTIR spectrophotometer, equipped with a Golden Gate Diamond ATR device, applying the reflectance technique (4000–300 cm^{-1}) and the peaks are reported in cm^{-1}. The electronic spectra were recorded using Perkin-Elmer Lambda 35 UV–vis spectrophotometer. X-band electron paramagnetic resonance (EPR) measurements were performed at room temperature in the solid state and at 77 K in the DMF solution on Bruker-EMX*plus* (DPPH is used as a standard, g = 2.0036). ^{1}H NMR spectra were recorded using a Bruker DPX 300 (300 MHz) spectrometer. Chemical shifts are reported as δ (ppm) values (multiplicity, integration, coupling constant J and assignment) relative to the dmso-d_6 solvent peak. Emission intensity measurements were carried out using a Shimadzu RF-5301PC spectrofluorophotometer equipped with a thermostatic bath. A circular dichroic spectrum of DNA or BSA was obtained by using JASCO J-716 spectropolarimeter.

Please cite this article in press as: S. Sangeetha, M. Murali, Int. J. Biol. Macromol. (2017), https://doi.org/10.1016/j.ijbiomac.2017.10.131

2.2. Synthesis of N-(2-quinolylmethylidene)aminophenol [H(quamol)]

A mixture of 2-quinolinecarboxaldehyde (1.57 g, 10 mmol) and 2-aminophenol (1.09 g, 10 mmol) was heated to reflux in anhydrous methanol (60 mL) for 4 h. After the solvent was removed under reduced pressure, 30 mL *n*-hexane-CH_2Cl_2 (V:V = 1:1) was then added, and the mixture was refluxed for another 0.5 h. The reaction mixture was filtered and left to stand at −20 °C overnight and bright yellow crystals were collected from the filtrate. Yield: 1.56 g, 63%. ^{1}H NMR (300 MHz, dmso-d_6) δ/ppm: 7.40 (d, 1H, 7.8, H_a), 7.16 (t, 1H, 8.4, H_b), 6.88 (t, 1H, 6.5, H_c), 6.96 (d, 1H, 7.8, H_d), 9.33 (s, 1H, —OH), 8.90 (s, 1H, —CH=N—), 8.56 (d, 1H, 7.6, H_1), 8.48 (d, 1H, 7.6, H_2), 8.11 (d, 1H, 8.2, H_3), 7.67 (t, 1H, 7.8, H_4), 7.82 (t, 1H, 7.6, H_5) and 8.04 (d, 1H, 7.2, H_6). Selected IR peaks (ν, cm^{-1}): 3471 b (ν_{O-H}), 3052 m (ν_{sC-H}), 2901 m (ν_{asC-H}), 1651 s ($\nu_{C=N}$)$_{azomethine}$, 1610 s ($\nu_{C=N}$)$_{quinoline}$, 1491, 1448 s ($\nu_{C=C}$)$_{quinoline}$, 1281 s (ν_{Ph-O}) and 988 w ($\nu_{-CH=N-}$). Anal. Cacld. For $C_{16}H_{12}N_2O$: C, 77.40; H, 4.87; N, 11.28. Found: C, 77.14; H, 4.98; N, 11.22%.

2.3. Synthesis of [Cu(quamol)Cl]·H_2O **1**

A methanol solution (15 mL) of $CuCl_2{\cdot}2H_2O$ (0.085 g, 0.5 mmol) was added dropwise to a yellow solution of H(quamol) (0.124 g, 0.5 mmol) in methanol (15 mL) with stirring for 2 h. The greenish brown solution obtained was filtered and the filtrate left to stand at 20 °C for slow evaporation. The crystalline dark brownish green solid formed after four days was collected by filtration. It is not suitable for X-ray structure determination. Yield: 0.108 g, 59%. Selected IR peaks (ν, cm^{-1}): 3342 b (ν_{O-H})$_{water}$, 3070 m (ν_{sC-H}), 2930 m (ν_{asC-H}), 1634 s ($\nu_{C=N}$)$_{azomethine}$, 1568 s ($\nu_{C=N}$)$_{quinoline}$, 1506, 1463 s ($\nu_{C=C}$)$_{quinoline}$, 1310 s (ν_{Ph-O}), 998 w ($\nu_{-CH=N-}$), 500 (ν_{Cu-N})$_{quinoline}$, 446 (ν_{Cu-N})$_{azomethine}$, 404 (ν_{Cu-O}) and 316 (ν_{Cu-Cl}). Anal. Cacld. For $C_{16}H_{13}N_2O_2ClCu$: C, 52.75; H, 3.60; N, 7.69. Found: C, 53.10; H, 3.13; N, 7.29%. Λ_M in aqueous DMF at 25 °C: 8 Ω^{-1} cm^2 mol^{-1}. ESI–MS in DMF solution: [Cu(quamol)Cl] displays a peak at *m*/*z* 346.6 (calcd. 346.3). Electronic absorption spectrum in DMF [λ_{max}/nm (ε_{max}/dm^3 mol^{-1} cm^{-1}): 608 (255), 434sh, 414 (2320), 313 (16580), 268 (20980)]. EPR spectrum in polycrystalline solid at RT: g_{iso} = 2.123. EPR spectrum in frozen DMF solution at 77 K: $g_{||}$ = 2.265, $A_{||}$ = 153 × 10^{-4} cm^{-1}, $g_{\perp}$ = 2.066, $g_{||}/A_{||}$ = 148 cm, *G* = 4.0.

2.4. DNA binding experiments

Solutions of DNA in the 5 mM Tris HCl/50 mM NaCl buffer gave a ratio of UV absorbances at 260 and 280 nm, A_{260}/A_{280}, of 1.9 [26], indicating that the DNA was sufficiently free of protein. Concentrated stock solutions of DNA (13.5 mol dm^3) were prepared in buffer and sonicated for 25 cycles, where each cycle consisted of 30 s with 1 min intervals. The concentration of DNA in nucleotide phosphate (NP) was determined by UV absorbance at 260 nm after 1:100 dilutions. The extinction coefficient, ε_{260}, was taken as 6600 dm^3 mol^{-1} cm^{-1}. Stock solutions were stored at 4 °C and used after no more than 4 days. Concentrated stock solutions of copper(II) complex was prepared by dissolving in 2% DMF/5 mM Tris-HCl/50 mM NaCl buffer at pH 7.1 and diluting suitably with the corresponding buffer to required concentrations for all the experiments. For absorption and emission spectral experiments, the DNA solutions were pretreated with solutions of copper(II) complex to ensure no change in concentrations of the copper(II) complex.

Absorption spectral titration experiments were performed by maintaining a constant concentration of the complex and varying the nucleic acid concentration. This was achieved by dissolving an appropriate amount of the metal complex and DNA stock solutions while maintaining the total volume constant (1 mL). This results in a series of solutions with varying concentrations of DNA, but with a constant concentration of the complex. The absorbance (*A*) of the most red-shifted band of the complex was recorded after successive additions of CT DNA.

Circular dichroic (CD) spectral experiments were done using a cylindrical 0.1 cm path length quartz cell. Each CD spectrum was collected after averaging over at least four accumulations using a scan speed of 100 nm min^{-1} and 1 s response time. Machine plus cuvette baselines were subtracted and the resultant spectrum zeroed outside the absorption bands.

For emission intensity measurements, the 2% DMF/5 mM Tris-HCl/50 mM NaCl buffer was used as a blank to make preliminary adjustments. The excitation wavelength was fixed and the emission range was adjusted before measurements. DNA was pretreated with ethidium bromide in the ratio [NP]:[EthBr] = 1:1 for 30 min at 27 °C. The metal complex was then added to this mixture and their effect on the emission intensity was measured.

Cyclic voltammetry (CV) and differential pulse voltammetry (DPV) were performed in a CHI 620C electrochemical analyzer at 25 ± 0.2 °C. The working electrode was a glassy carbon disk (0.0707 cm^2) and the reference electrode, a saturated calomel electrode. A platinum wire was used as the counter electrode. The supporting electrolyte was 2% DMF/5 mM Tris-HCl/50 mM NaCl buffer (pH 7.1). Solutions were deoxygenated by purging with nitrogen gas for 15 min prior to measurements; during measurements a stream of N_2 gas was passed over them. The redox potential $E_{1/2}$ was calculated from the anodic (E_{pa}) and cathodic (E_{pc}) peak potentials of CV traces as (E_{pa} + E_{pc})/2 and also from the peak potential (E_p) of DPV response as E_p + ΔE/2 (ΔE is the pulse height).

2.5. Protein binding experiments

The stock solution of protein (1.0 × 10^{-4} mol L^{-1}) was prepared by dissolving the solid BSA in 0.05 M phosphate buffer at pH 7.4 and stored at 0–4 °C in the dark for about a week and then diluted to 1.0 × 10^{-6} mol L^{-1} using phosphate buffer (pH 7.4, 0.05 M) when used. The concentration of BSA was determined from optical density measurements, using the value of molar absorptivity of ε_{280} = 44720 M^{-1} cm^{-1} [20]. All fluorescence measurements were performed using a 10 mm quartz cuvette at two different temperatures (300 and 310 K).

Quantitative analyses of the interaction between complex and BSA were performed by fluorimetric titration (0.05 M phosphate buffer, pH 7.4). A 3.0 mL portion of an aqueous solution of BSA was titrated by successive additions of the complex. Titrations were done manually by using an Eppendorf micro-pipette. For every addition, the mixture solution was shaken and allowed to stand for 20 min at the corresponding temperature (300 and 310 K) and then the fluorescence intensities were measured with an excitation wavelength of 280 nm and emission wavelengths in the interval 290–500 nm. No correction for the inner filter effect was applied since complex represented very low absorbance (less than 0.1) at excitation and emission wavelengths. The excitation and emission slit width (each 5.0 nm), scan rate (fast) were constantly maintained for all the experiments. In the meantime, the synchronous fluorescence intensity of the mixed solution was measured by setting the excitation and emission wavelength interval ($\Delta\lambda$) at 15 and 60 nm. The UV–vis absorption spectra of 1.0 μM free BSA as well as BSA/complex (equal molar ratio) in 0.5 M phosphate buffer of pH 7.4 were recorded from 200 to 500 nm. The far-UV CD measurements of BSA (1.0 μM) in the absence and presence of copper(II) complex (1:0.1, 1:0.2, 1:0.3) were recorded from 200 to 260 nm in 0.05 M phosphate buffer (pH 7.4) at room temperature.

Please cite this article in press as: S. Sangeetha, M. Murali, Int. J. Biol. Macromol. (2017), https://doi.org/10.1016/j.ijbiomac.2017.10.131

2.6. DNA cleavage experiments

The cleavage of DNA in the absence and presence of an activating agent such as ascorbic acid (10 or 20 μM) was monitored using agarose gel electrophoresis. A typical reaction mixture, containing ϕX174 supercoiled phage DNA (form I, 20 μM) and copper(II) complex in 2% DMF–5 mM Tris-HCl–50 mM NaCl buffer at 7.1 was incubated at 37 °C. After the incubation period, the reaction was quenched by keeping the samples at −20 °C, followed by the addition of loading buffer (0.025 mg bromophenol blue, 1 mL glycerol and 1 mL MilliQ water). This was then loaded on a 1% agarose gel containing ethidium bromide (2.54 μM in the gel as well as in the buffer). The gels were run at a constant voltage of 40 V for 3 h in the 1 × TAE buffer containing ethidium bromide. After washing with distilled water, the gels were visualized under a UV transilluminator and the bands were documented and quantified using a BioRad Gel Doc 1000 apparatus interfaced with a computer. The cleavage efficiency was measured by determining the ability of the complex to convert the supercoiled DNA (SC, Form-I) to nicked circular form (NC, Form-II) and linear form (LC, Form-III). Inhibition reactions were carried out by prior incubation of the SC ϕX174 DNA (20 μM) with superoxide dismutase (0.5 units), DMSO (20 μM) and sodium azide (100 μM).

2.7. Cytotoxicity assays

Cytotoxicity was estimated by the microculture sulforhodamine B (SRB) test [27]. For the cytotoxicity evaluation in the human cancer cell lines MCF7, EVSA-T, WIDR, IGROV, M19 MEL, A498 and H226 and a normal cell line NIH 3T3, the test (**1**), H(quamol) and reference compounds were dissolved to a concentration of 250.000 μg/mL in full medium, by 20 fold dilution of a stock solution which contained 1 mg compound/200 μL DMSO (Sigma, St. Louis MO, USA). Trypsinized tumor cells (150 μL, containing $1.5–2.0 \times 10^3$ cells/well) were plated in 96-wells flat bottom microtiter plates (Cellstar, Greiner Bio-one). The plates were pre-incubated for 48 h at 37 °C, 5.5% CO_2. A three-fold dilution sequence of ten steps was made in full medium, starting with 250.000 μg/mL stock solution. Every dilution was used in quadruplicate by adding 50 μL to a column of four wells, resulting in a higher concentration of 62.500 μg/mL. The plates were incubated for 7 days, after which the cells were fixed with 10% trichloroacetic acid in PBS buffer (NPBI BV, Emmer-Compascuum, NL) and placed at 4 °C for 1 h. After three washings with water, the cells were stained for at least 15 min with 0.4% SRB (Sigma, St. Louis MO, USA) dissolved in 1% acetic acid. The cells were washed with 1% acetic acid to remove the unbound stain. The plates were air-dried and the bound stain was dissolved in 150 μL of 10 mM Tris-base (unbuffered). The value of A540 was assessed using an automated microplate reader (Labsystems Multiskan MS). Data were used for concentration-response curves and the determination of the ID_{50} values using Deltasoft 3 software (Biometallics Inc., Princeton, NJ, USA) [28]. Subsequent conversion of units provided the IC_{50} values for all samples tested.

3. Results and discussion

3.1. Synthesis and spectral properties

The condensation reaction of 2-aminophenol with quinoline-2-carboxaldehyde leads to the new phenol-imine tridentate ligand H(quamol). A new singlet observed at 8.90 ppm in the ^{1}H NMR spectrum of the ligand corresponds to the azomethine (—CH=N—) proton, which confirmed the condensation of 2-aminophenol and quinoline-2-carboxaldehyde. Another singlet observed at 9.33 ppm is attributable to the phenolic —OH proton of 2-aminophenol. Also,

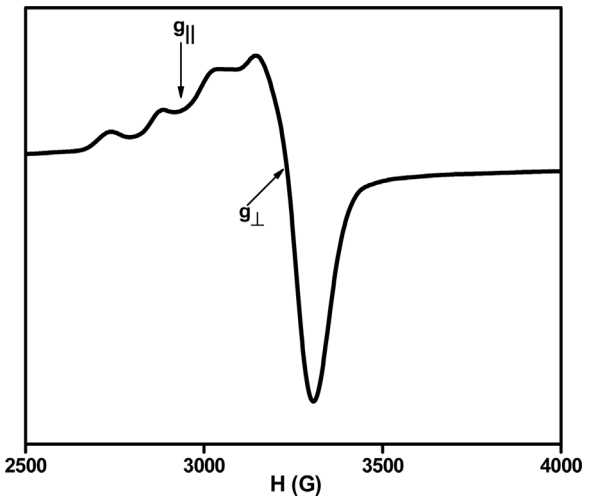

Fig. 2. EPR spectrum of **1** in DMF solution at 77 K (Microwave frequency: 9.137 GHz).

two sets of NMR signals observed in the range 6.88–7.40 (phenolic, H_a–H_d) and 7.67–8.56 ppm (quinolyl, H_1–H_6) can be ascribed to the aromatic protons. The infrared spectrum of H(quamol) shows a broad band around 3471 cm^{-1}, an intense band around 1651 cm^{-1} and a medium intensity band around 1281 cm^{-1}, which is assigned to $\nu_{O–H}$, $\nu_{C=N}$ and $\nu_{Ph–O}$ respectively. The copper(II) complex was isolated by treating copper(II) chloride dihydrate with the H(quamol) ligand in equimolar quantities in methanol as solvent. Based on elemental analysis the complex was formulated as [Cu(quamol)Cl]·H_2O and found to be stable in solution phase, as the ESI–MS data (m/z, 346.6 in DMF) supports the existence of the complex [Cu(quamol)Cl]. This is substantiated by conductivity measurements in aqueous DMF solution (Λ_M, 8 Ω^{-1} cm^2 mol^{-1}), which is expected for a nonelectrolyte in solution. Despite repeated attempts to recrystallize **1** by vapour diffusion of ethanol into DMF, good quality crystals of **1** are not obtained.

The absence of the infrared band near 3471 cm^{-1} due to $\nu_{O–H}$ and the in-plane deformation, and the shift of ligand $\nu_{Ph–O}$ at 1281 cm^{-1} to 1310 cm^{-1} indicate the deprotonation and coordination of the phenolate oxygen of H(quamol). However, the broad band centered around 3342 cm^{-1} due to $\nu_{O–H}$ reveal the presence of water of crystallization [29], which is in accordance with the results of elemental analysis. Upon coordination, the ligand $\nu_{C=N}$ (1651 cm^{-1}) is shifted to 1634 cm^{-1} ($\Delta\nu$, 17 cm^{-1}), suggesting the involvement of azomethine nitrogen in coordination to copper(II). The bands observed around 1448, 1491 and 1610 cm^{-1} characteristic of quinolyl moiety are shifted to 1463, 1506 and 1568 cm^{-1} in **1** revealing the coordination of quinolyl nitrogen to copper(II). The low intensity peaks observed at 500, 446 and 404 cm^{-1} can be assigned respectively to ν_{Cu-N} (quinoline), ν_{Cu-N} (azomethine) and ν_{Cu-O} (phenolate) vibration. Also, **1** displays a band at 316 cm^{-1}, characteristic of ν_{Cu-Cl} [30].

In DMF solution, **1** exhibits only one broad band (608 nm) in the visible region, typical of ligand field (LF) absorption for Cu(II) located in a tetragonal field. The higher energy bands observed around 414 and 313 nm are assigned to $PhO^- \rightarrow Cu(II)$ and $Cl^- \rightarrow Cu(II)$ ligand-to-metal charge transfer (LMCT) transitions [31] respectively. The intense absorption band around 268 nm is attributed to the intraligand $\pi \rightarrow \pi^*$ transition [32].

The polycrystalline EPR spectrum of **1** is isotropic, while the frozen-solution spectrum is axial (Fig. 2) with line shapes [$g_{||} > g_{\perp} > 2.0$, $G = (g_{||} - 2)/(g_{\perp} - 2) = 4.0$] [27] characteristic of mononuclear copper(II) complex, suggesting the presence of $d_{x^2-y^2}$ ground state for Cu(II) located in a square based environment [31]. A square-based CuN_4 chromophore is expected [33,34] to show

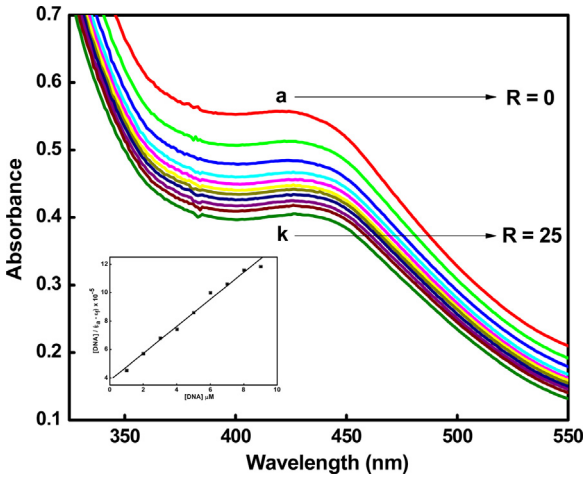

Fig. 3. Absorption spectra of **1** (75×10^{-6} M) in 2% DMF/5 mM Tris-HCl/50 mM NaCl buffer at pH 7.1 in the absence (R = 0) and presence (R = 10) of increasing amounts of CT DNA. Inset: Plot of [DNA] *vs* [DNA]/($\varepsilon_a - \varepsilon_f$) at R = 10 of **1**.

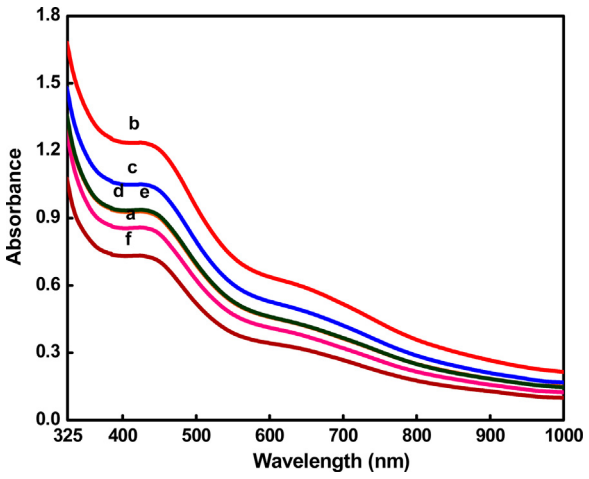

Fig. 4. Absorption spectra of **1** (4×10^{-3} M) (a) in 2% DMF/5 mM Tris-HCl/50 mM NaCl buffer at pH 7.1, on interacting with N-methylimidazole (b), guanosine-5′-monophosphate (c), adenosine-5′-monophosphate (d), cytosine-5′-monophosphate (e) and CT DNA (f) at $R = 4$.

a $g_{||}$ value of 2.200 and $A_{||}$ value of 180–200 $\times 10^{-4}$ cm^{-1} and the replacement of two nitrogen atoms in this chromophore by an oxygen atom and chloride ion, is expected to enhance the $g_{||}$ value and decrease the $A_{||}$ value. Thus, **1** possesses a higher $g_{||}$ (2.265) and appreciably lower $A_{||}$ (153×10^{-4} cm^{-1}) values characteristic of CuN_2OCl chromophore, which are comparable with its benzimidazolyl analogues {[Cu(L1)Cl] **2**: $g_{||}$, 2.272 and $A_{||}$, 166×10^{-4} cm^{-1}; [Cu(L2)Cl] **3**: $g_{||}$, 2.270 and $A_{||}$, 169×10^{-4} cm^{-1} where H(L1) is 2-(2-(1H-benzimidazol-2-yl)ethyliminomethyl)phenol and H(L2) is 2-(2-(1H-benzimidazol-2-yl)ethyliminomethyl)-4-methylphenol} [35]. The Cu(II) complexes with perfectly square planar geometry, the $g_{||}/A_{||}$ quotient [36] ranges from 105 to 135 cm and for **1** the value of $g_{||}/A_{||}$ quotient, 148 cm [$g_{||}/A_{||}$, 137 (**2**); 134 cm (**3**)] reflecting the presence of distortion in CuN_2OCl chromophore imposed by the bulky quinolyl moiety.

3.2. DNA binding studies

As the primary pharmacological target is DNA for many antitumor drugs, the study of binding of metal complexes to DNA is of paramount importance for the development of effective chemotherapy metal-based drugs. Therefore, the absorption spectra of **1** in the absence and presence of DNA at different concentrations (R = [DNA]/[complex] = 1–10) in 2% DMF/5 mM Tris-HCl/50 mM NaCl buffer (pH = 7.1) were recorded (Fig. 3) at 424 nm ($PhO^- \rightarrow Cu(II)$ LMCT transition). With an increase in concentration of CT DNA, the hypochromism of 27.0% and red-shift of 3 nm for **1** were observed whereas its benzimidazolyl analogues showed less hypochromism (**2**, 12.0; **3**, 8.0%) with no red-shift [35]. The value of intrinsic equilibrium DNA binding constant [K_b, 2.48×10^5 (**1**); 10.0×10^3 (**2**); 8.0×10^3 M^{-1} (**3**)] [35] suggests the enhanced DNA binding propensity of **1** compared to **2** and **3**, possibly due to the involvement of partial intercalative interaction of planar quinolyl ring into the DNA base pairs leading to high hypochromism.

It may be expected that the labile chloride ion of the complex can be replaced by a nucleophile on DNA, usually a nitrogenous base such as guanine N7, leading to a strong covalent bonding of the complex with DNA [37]. In order to explore these possibility of **1** forming a coordinate bond with DNA through the displacement of the equatorially coordinated chloride anion [38], the ligand field (LF) band of the complex has been monitored (Table 1) with the addition of potential small ligands like *N*-methylimidazole (Meim) and the nucleotides guanosine-5′-monophosphate (GMP), adenosine-5′-monophosphate (AMP) and cytosine-5′-monophosphate (CMP) (Fig. 4). With the addition of GMP, the visible band of **1** is blue-shifted (~10 nm) with an increase in absorptivity. A similar but lower blue-shift (~7 nm) and a small increase in absorptivity are observed with the addition of AMP. On the other hand, addition of Meim and CMP does not effect any spectral change at all. The spectral changes observed for GMP and AMP are considerably less, indicating weaker coordination of N7 atom of GMP and AMP to copper(II). However, the addition of DNA to **1** causes a red-shift (~2 nm) in the LF band with a decrease in absorptivity revealing that **1** does not form a covalent bond on interaction with DNA in view of the distorted square-planar structure of the complex. So it is clear that chloride anion is not labile (cf. above) and is not replaced by guanine N7.

The observed CD spectrum of CT DNA (2×10^{-5} M) consists of a positive band (277 nm) due to base stacking and a negative band (245 nm) due to helicity (Fig. S1), which is characteristic of DNA in the right-handed B form [39]. The simple groove binding and electrostatic interaction of small molecules with DNA shows less or no perturbations on the base stacking and helicity bands, while intercalation enhances the intensities of both the bands stabilizing the right-handed B conformation of DNA [40]. When **1** is incubated with DNA at 1/R (=[Cu complex]/[DNA]) value of 3, the CD spectrum of DNA (Fig. S1) undergoes changes in both positive (20% increase in intensity) and negative bands (45% decrease in intensity, 5 nm red-shift), which is consistent with partial intercalative interaction of quinolyl ring, supporting the results from UV–vis spectroscopy.

The fluorescence intensity of EthBr bound to DNA at 610 nm (λ_{ex}, 520 nm) shows a remarkable decrease with the addition of **1** (Fig. 5), indicating DNA-bound EthBr molecules are released into solution [41]. Such fluorescence quenching may be caused by the strong partial intercalative interaction of **1** (cf. above), leading to the displacement of DNA-bound EthBr. Also, it may be seen that the fluorescence quenching follows Stern-Volmer behavior (Fig. 5, Inset) [42]. The apparent DNA binding constant (K_{app}) is calculated [43] using the equation, K_{EthBr}[EthBr] = K_{app}[complex], where K_{EthBr} is 4.94×10^5 M^{-1} [44], the concentration of EthBr is 1.25×10^{-6} M and the concentration of the complex is that used to obtain a 50% reduction of fluorescence intensity of EthBr. The apparent DNA binding constant (K_{app}, 7.72×10^4 M^{-1}) value is consistent with the K_b value obtained by UV–vis absorption spectral study.

Typical cyclic voltammetric (CV) responses for **1** in 2% DMF–5 mM Tris-HCl–50 mM NaCl buffer (pH = 7.1) in the absence and presence of CT DNA are shown in Fig. S2. The cathodic

Table 1
Ligand field spectral properties of **1** on binding to CT DNA[a] and other small molecules[b–e].

	λ_{max} (nm)	$\Delta\lambda_{max}$ (nm)	$\Delta\varepsilon$ (%)	Change in absorbance (Shift)
1	610	–	–	–
1 + CT DNA	612	2	17	Hypochromism (Red)
1 + Meim	610	0	12	Hyperchromism
1 + GMP	600	10	57	Hyperchromism (Blue)
1 + AMP	603	7	30	Hyperchromism (Blue)
1 + CMP	610	0	12	Hyperchromism

[a] R = [DNA]/[**1**] = 4, concentration of copper solution = 4×10^{-3} M.
[b] R = [Meim]/[**1**] = 4, concentration of copper solution = 4×10^{-3} M
[c] R = [GMP]/[**1**] = 4, concentration of copper solution = 4×10^{-3} M.
[d] R = [AMP]/[**1**] = 4, concentration of copper solution = 4×10^{-3} M.
[e] R = [CMP]/[**1**] = 4, concentration of copper solution = 4×10^{-3} M.

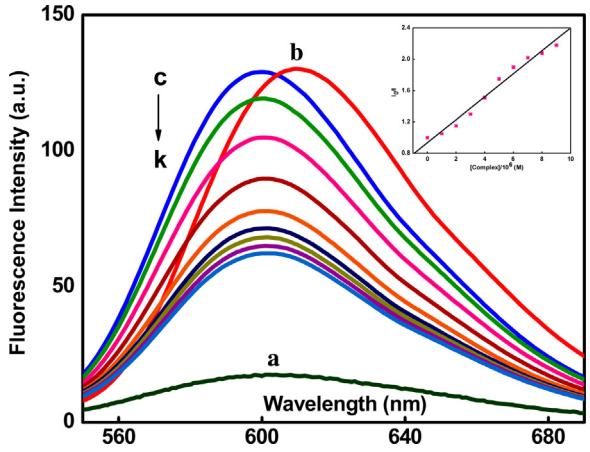

Fig. 5. Fluorescence quenching curves of ethidium bromide bound to DNA in 2% DMF/5 mM Tris-HCl/50 mM NaCl buffer at pH 7.1: (a) EthBr (1.25 μM); (b) EthBr + DNA (125 μM); (c–k) EthBr + DNA + **1** (0–9 μM). Inset: Plot of [complex × 10^{-6}] *vs* I_0/I of **1**.

(−0.694 V) and anodic peak potential (−0.414 V) values observed for **1** correspond to Cu^{II}/Cu^{I} redox couple [45]. The high separation of the cathodic and anodic peak potential (ΔE_p, 280 mV) indicates the poor electrochemical reversibility of the Cu^{II}/Cu^{I} couple. Upon addition of DNA, the cathodic current decreases significantly, which is expected of strong binding of the complex with DNA [46]. For a Nernstian electron transfer system, in which both the oxidized and reduced forms associate with DNA in solution, differential pulse voltammetry (DPV) can be used to calculate the corresponding equilibrium constants for each oxidation state according to the equation [46], $E^{0'}{}_b - E^{0'}{}_f = 0.059\log(K_+/K_{2+})$, where $E^{0'}{}_b$ and $E^{0'}{}_f$, the formal potentials of Cu^{II}/Cu^{I} couple in the bound and free forms, respectively, K_{2+} and K_+ are the binding constants of oxidized and reduced forms to DNA, respectively. The formal potentials of Cu^{II}/Cu^{I} couple in the free ($E^{0'}{}_f$, −0.571 V) and DNA-bound ($E^{0'}{}_b$, −0.616 V) forms shift negatively (−45 mV) after reacting with DNA. The ratio of the binding constants (K_+/K_{2+}) of the Cu(I) and Cu(II) form of DNA is calculated to be 0.2, indicating that Cu(II) form binds to DNA more strongly than Cu(I) form [47].

3.3. Protein binding studies

The fluorescence of BSA is caused by three intrinsic characteristics of the protein, namely tryptophan, tyrosine and phenyl alanine residues, among them; tryptophan and tyrosine are the dominant intrinsic fluorophores. Fluorescence quenching refers to any process that decreases the fluorescence intensity from a fluorophore due to a variety of molecular interactions, including excited-state reactions, molecular rearrangements, energy transfer ground-state complex formation and collisional quenching. Thus, the emission

Table 2
Quenching, association, binding and thermodynamic parameters of the interaction of **1** with BSA at different temperatures.[a]

Parameters	300 K	R	310 K	R
K_{SV} (10^5 M^{-1}) ± SD	2.59 ± 0.003	0.9997	3.24 ± 0.004	0.9991
K_q (10^{13} M^{-1} s^{-1})	2.59		3.24	
K_b (10^5 M^{-1}) ± SD	6.13 ± 0.061	0.9983	8.73 ± 0.047	0.9993
n ± SD	1.05 ± 0.01		1.08 ± 0.01	
ΔH (kJ mol^{-1})	77.671			
ΔS (J mol^{-1} K^{-1})	109.383		110.071	
ΔG (kJ mol^{-1})	−32.737		−34.044	

[a] R is the linear correlated coefficient.

spectra of BSA (λ_{em}, 340 nm; λ_{ex}, 280 nm) in the presence of increasing concentrations of **1** were recorded at 300 K and 310 K. The fluorescence intensity of BSA decreased regularly (Fig. 6), up to 67.8% (300 K) and 70.8% (310 K), accompanied by a hypsochromic shift of 7 nm. The Stern-Volmer plots (Fig. S3) are linear (K_{SV}: 300 K, 2.59; 310 K, 3.24×10^5 M^{-1}) and quenching rate constant (k_q) is on the order of 10^{13} M^{-1} s^{-1}, which is 1000-fold higher than the maximum limit (2.0×10^{10} M^{-1} s^{-1}) [48]. On the other hand, upon addition of **1** to BSA results in an increase in the intensity of the absorption band of BSA at 278 nm (Fig. S4), indicating that more aromatic acid residues were extended into the aqueous environment and the tertiary structure of BSA was destroyed [49]. These results show that the interaction between **1** and BSA is static due to the formation of a non-fluorescent BSA-**1** compound. The binding constant K_b is directly correlated (Fig. S5) with temperature (300 K, 6.13; 310 K, 8.73×10^5 M^{-1}), which indicates the formation of stable BSA-**1** compound and the number of binding site n is equal to one corresponds to the existence of just a single binding site. So, the results suggest that the complex binds to the hydrophobic pocket located in subdomain IIA [50]. As shown in Table 2, a negative value of ΔG identifies the spontaneity of the interaction. The positive values obtained for both ΔH and ΔS indicates that a hydrophobic association is the major binding force and that the interaction is entropy driven process [51]. In addition to hydrophobic interaction, a possible covalent bonding may be also considered. However, the value of ΔH obtained here (78 kJ mol^{-1}) is considerably below what would be expected for a covalent bond formation (≥120 kJ mol^{-1}) [52].

According to the theory of Miller [53], when $\Delta\lambda$ between excitation wavelength and emission wavelength is set at 15 or 60 nm, the synchronous fluorescence offers characteristic information on the environment of tyrosine and tryptophan residues, respectively. The synchronous fluorescence spectra of BSA with various amounts of **1** were recorded at $\Delta\lambda$ = 15 nm and $\Delta\lambda$ = 60 nm. Upon addition of **1** (Fig. S6), the emission maxima of tyrosine and tryptophan residues have significant blue-shifted (tyrosine: 313–309; tryptophan, 346–345 nm). The blue-shift effect expresses the change in conformation of BSA; the polarity around the tyrosine and tryptophan residue decreases and the hydrophobicity increased. For

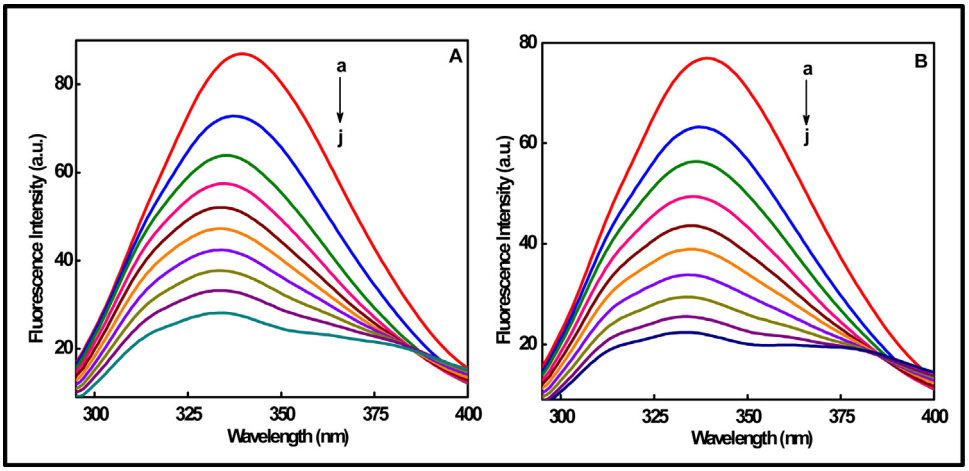

Fig. 6. Changes in the fluorescence spectra of BSA through the titration with complex **1** at 300 K (left, **A**) and 310 K (right, **B**). The concentration of BSA is 1×10^{-6} M, and the concentration of **1** was varied from (a) 0.0 to (j) 4.0×10^{-6} M; pH 7.4 and λ_{ex} 280 nm.

BSA-**1** system, the synchronous fluorescence quenching ratios, R_{SFQ} at $\Delta\lambda = 60$ nm (73.5%) is greater than the corresponding one for $\Delta\lambda = 15$ nm (58.8%; Fig. S7), indicating that **1** reached sub-domain IIA, where the only one Trp 212 residues on BSA was located.

The distance between the buried Trp-212 (as donor) and the interacted complex (as acceptor) was estimated by Förster's non-radiative energy transfer theory and the overlapping of the fluorescence spectrum of BSA with absorption spectrum of **1** was shown in Fig. S8. According to the Förster's equations, we obtain that $J(\lambda) = 2.04 \times 10^{14}\ M^{-1}\ cm^3$, $R_0 = 2.84$ nm, $E = 0.18$ and $r = 3.16$ nm. The donor (Trp 212 in BSA) to acceptor (**1**) distance (r) is less than 8 nm [54], indicating that the non-radiative energy transfer from BSA to **1** occurred with high probability.

To ascertain the possible influence of **1** binding on the secondary structure of BSA, we have performed far-UV CD spectroscopy of BSA in the absence and presence of **1**. BSA has a characteristic strong double minimum signal (208 and 222 nm) [55] contribute to the $n \rightarrow \pi^*$ transfer of the peptide bond of the α-helix. The intensities of double minimum reflect that BSA contains more than 50% of α-helical structure. The CD spectral (Fig. S9) data reveal the decrease in α-helix structure of BSA (BSA to **1** molar ratio, % of α-helix at 208 and 222 nm respectively: 1:0, 63.8 and 60.2%; 1:0.1, 60.4 and 57.8%; 1:0.2, 58.4 and 57.1%; 1:0.3, 54.6 and 51.7%), indicating that **1** bound with the amino acid residue of the polypeptide chain of BSA and destroys their hydrogen bonding networks. Nevertheless, the CD spectra of BSA in the presence and absence of **1** were similar in shape, implying that the structure of BSA after binding of **1** continues to be predominant α-helical.

3.4. DNA cleavage

The ϕX174 phage DNA (20 μM in base pairs) and **1** (10–100 μM) is incubated for 1 h at 37 °C in a medium 2% DMF/5 mM Tris-HCl/50 mM NaCl buffer (pH = 7.1), with ascorbic acid (10 μM) as an activating agent. When the reaction mixture is subjected to electrophoresis, the fastest migration will be observed in the supercoiled form (SC, Form I). If one strand is cleaved, the supercoils will relax to produce a slow-moving nicked circular form (NC, Form II). If both strands are cleaved, a linear form (LC, Form III) will be generated which migrates between SC and NC forms. The activity of **1** is assessed by the conversion of DNA from SC to NC and LC. The results of the gel electrophoresis separations of the reaction mixture are depicted in Fig. 7. Under identical conditions, no cleavage of ϕX174 DNA occurred for ascorbic acid (lane 2) or copper(II) complex alone. It was found that at a complex concentration of 10 μM converts SC DNA into 70% NC form (lane 3). When the complex concentration is increased in the presence of an activator, the amount of Form I decreases gradually and Form II increases (lane 4 – lane 12). It was revealed that **1** is capable of cleaving supercoiled form of ϕX174 DNA (Form I) into nicked circular form (Form II) but not linear form (Form III). At a complex concentration of 80 μM, it causes complete conversion of SC to NC (97%) form (lane 10), revealing that the cleavage of ϕX174 DNA is highly concentration dependent. When the concentration of ascorbic acid is increased from 10 μM to 20 μM, at 20 μM complex concentration cleaves SC DNA into 80% NC and 20% LC form while at 80 μM complex concentration converts SC form into 65% NC and 35% LC (Fig. S10) form.

The time-dependent cleavage of DNA by **1** is also studied under similar conditions ([complex] = 80 μM and [DNA] = 20 μM in bp). With the reaction time is increased, the amounts of NC form increases and SC form gradually disappears (Fig. 8A). Also, the appearance of NC form as well as the disappearance of SC form follow pseudo-first-order kinetic profiles and fit well into a single-exponential decay curve (Fig. 8B). When the experimental data were fit, the rate constant, $k_{obs} = \sim 0.0373\ min^{-1}$ and the half-life time, $t_{1/2} = \sim 18.58$ min was obtained. Previous studies showed that an oxidative process for the SC to NC conversion, which follows a second order profile [56]. Taking this as a precedent, we established the rate law as $\delta[DNA_{SC}]/\delta t = -k[complex][DNA_{SC}]$, where $[DNA_{SC}]$ represents the portion of supercoiled DNA, t is the time and k is the second order kinetic constant. From this equation we obtain a value for $k = \sim 2.4 \times 10^4\ M^{-1}\ min^{-1}$, which is higher than those for other copper(II) complexes in oxidative cleavage with ascorbic acid [56]. The high value of the second order constant k suggests a very strong interaction of the complex with DNA.

To verify the involvement of reactive oxygen species (ROS), which may be formed in the DNA cleavage reaction, DNA cleavage experiments were carried out in the presence of hydroxyl radical scavenger (DMSO) [57], superoxide scavenger (SOD) [58] and singlet oxygen quencher (NaN_3) [59] under physiological conditions. As shown in Fig. 9, no obvious inhibition of DNA cleavage is observed in the presence of DMSO, NaN_3 and SOD, which indicate the absence of hydroxyl radical, singlet oxygen and superoxide in the cleavage reaction and that the DNA cleavage promoted by the complex might occur *via* copper-oxygen species. We propose that, in the first step, the complex (quamol)Cu(II) is reduced by ascorbic acid to form the (quamol)Cu(I) species. The (quamol)Cu(I) reacts with O_2 to generate superoxide anion ($O_2^{\bullet -}$) and subsequently H_2O_2. The (quamol)Cu(I) formed and bound to DNA forming the (DNA)(quamol)Cu(I) adduct, which reacts with H_2O_2

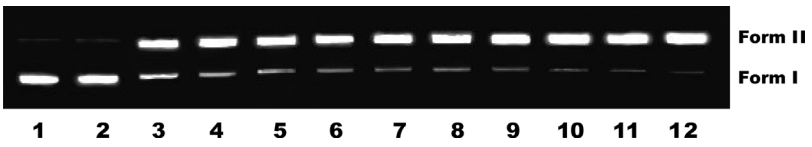

Fig. 7. Gel electrophoresis diagram showing the cleavage of ϕX174 DNA (20 μM) by **1** in a 2% DMF/5 mM Tris-HCl/50 mM NaCl buffer at pH 7.1 and 37 °C in the presence of ascorbic acid (AA; 10 μM) with an incubation time of 1 h: lane 1, DNA control; lane 2, DNA + AA; lane 3, DNA + **1**(10 μM) + AA; lane 4, DNA + **1**(20 μM) + AA; lane 5, DNA + **1**(30 μM) + AA; lane 6, DNA + **1**(40 μM) + AA; lane 7, DNA + **1**(50 μM) + AA; lane 8, DNA + **1**(60 μM) + AA; lane 9, DNA + **1**(70 μM) + AA; lane 10, DNA + **1**(80 μM) + AA; lane 11, DNA + **1**(90 μM) + AA; lane 12, DNA + **1**(100 μM) + AA.

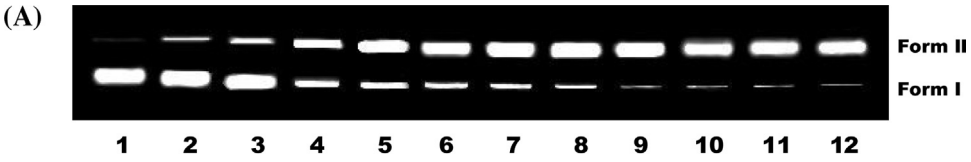

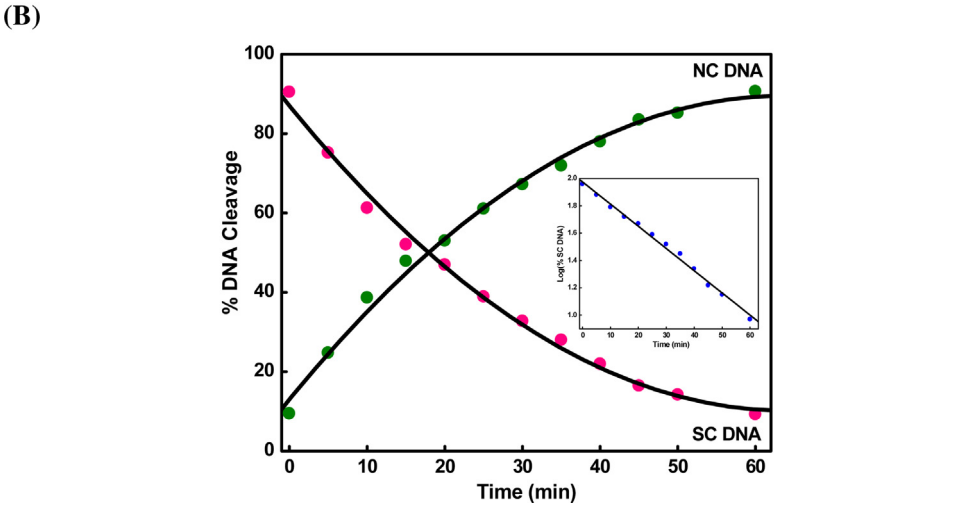

Fig. 8. (A) Time course of supercoiled ϕX174 DNA (20 μM) cleavage by **1** (80 μM) in a 2% DMF/5 mM Tris-HCl/50 mM NaCl buffer at pH 7.1 and 37 °C in the presence of ascorbic acid (AA; 10 μM) with an incubation times of 0, 5, 10, 15, 20, 25, 30, 35, 40, 45, 50 and 60 min for lanes 1–12. (B) Plot of the increase in NC form with time and plot of the decrease in SC form with time. Inset: Plot of log(% SC DNA) *vs* time.

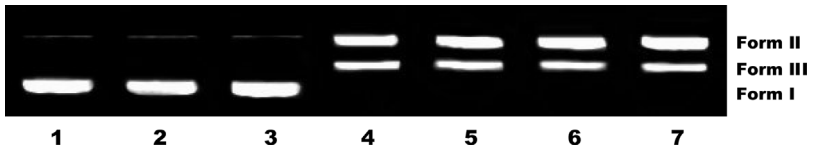

Fig. 9. Gel electrophoresis diagram showing the cleavage of ϕX174 DNA (20 μM) by **1** (80 μM) in a 2% DMF/5 mM Tris-HCl/50 mM NaCl buffer at pH 7.1 and 37 °C in the presence of ascorbic acid (AA; 20 μM) with an incubation time of 2 h: lane 1, DNA control; lane 2, DNA + AA; lane 3, DNA + **1**; lane 4, DNA + **1** + AA; lane 5, DNA + **1** + AA + SOD (0.5 units); lane 6, DNA + **1** + AA + NaN_3 (100 μM); lane 7, DNA + **1** + AA + DMSO (20 μM).

to produce free hydroxide ion and DNA bound Cu(II)-hydroxyl radical intermediate [60]. The latter forms a DNA bound copper-oxene or a resonance hybrid of a DNA bound copper(II)-hydroxyl radical and a putative copper(III)-oxene/copper(III)-hydroxo species, which generates a deoxyribose-centered radical by C-1/C-4 hydrogen abstraction [61–63].

3.5. Cytotoxicity studies

The cytotoxicity of H(quamol) and **1** against seven human tumor cell lines of different cancer origins, *viz.* renal cancer (A498), breast cancer (EVSA-T and MCF7), non-small cell lung cancer (H226), ovarian cancer (IGROV), melanoma (M19 MEL) and colon cancer (WIDR) are investigated in comparison with six known anticancer drugs, *viz.* doxorubicin (DOX), cisplatin (CPT), 5-fluorouracil (5-FU), methotrexate (MTX), etoposide (ETO) and taxol (TAX) under identical conditions by using SRB test (Table 3). Indeed, a ligand or complex with IC_{50} values higher than 10 μM is considered to be inactive [64]. The test results indicate that H(quamol) is inactive (IC_{50}, 92 to >100 μM) to all the cancer cell lines. However, chelation of H(quamol) with copper(II) dramatically enhances the cytotoxicites of cancer cell lines. Thus, the cytotoxicities of **1** are highly active against M19 MEL (IC_{50}, 2.018 μM) and EVSA-T (IC_{50}, 3.802 μM) and moderate for MCF7 (IC_{50}, 7.576 μM) while low or no activity for H226 (IC_{50}, 12.732 μM), IGROV (IC_{50}, 23.001 μM), A498 (IC_{50}, 23.360 μM) and WIDR (IC_{50}, 24.664 μM) cancer cell lines. The cell killing activity of **1** against cancer cell lines is much higher than that of the free ligand, which may be attributed to the

Table 3
In vitro cytotoxicity assays for H(quamol), **1**, doxorubicin (DOX), cisplatin (CPT), 5-fluorouracil (5-FU), methotrexate (MTX), etoposide (ETO) and taxol (TAX) screened against seven human tumor cell lines of different origins, *viz.* renal cancer (A498), breast cancer (EVSA-T and MCF7), non-small cell lung cancer (H226), ovarian cancer (IGROV), melanoma (M19 MEL) and colon cancer (WIDR) and a normal cell line, mouse embryonic fibroblasts (NIH 3T3).

Drug[a] (IC_{50}/μM using SRB as cell viability test)								
Cell lines	H(quamol)	**1**	DOX	CPT	5-FU	MTX	ETO	TAX
A498	>100.000	23.360	0.166	7.509	1.099	0.081	1.803	<0.004
EVSA-T	93.674	3.802	0.015	1.406	3.651	0.011	0.435	<0.004
H226	94.126	12.732	0.366	10.895	2.613	5.033	5.397	<0.004
IGROV	>100.000	23.001	0.110	0.563	2.283	0.015	0.780	<0.004
M19 MEL	92.247	2.018	0.029	1.860	3.397	0.051	0.693	<0.004
MCF7	94.008	7.576	0.018	2.330	5.764	0.040	3.551	<0.004
WIDR	>100.000	24.664	0.020	3.223	1.729	<0.007	0.206	<0.004
NIH 3T3	>100.000	>100.000	–	–	–	–	–	–

[a] IC_{50} = concentration of drug required to inhibit growth of 50% of the cancer cells.

extended planar structure of quinolyl ring. Interestingly, **1** exhibits a potency comparable to cisplatin, but approximately 1.5 times more active than 5-fluorouracil in M19 MEL melanoma cancer cell line, indicating that **1** has the potential to act as an effective metal-based anticancer drug. The IC_{50} values obtained with **1** are higher compared to ones with cisplatin or 5-fluorouracil in MCF7 breast cancer cell line. However, for EVSA-T breast cancer cell line, the cytotoxic activity of **1** is slightly higher than cisplatin, but more or less equal to 5-fluorouracil. In all cell lines, the cytotoxicities of **1** are even higher than those reached with doxorubicin or methotrexate or etoposide or taxol. Moreover, it was non-toxic to healthy mouse embryonic fibroblasts (NIH 3T3) cells up to the higher concentration tested (IC_{50}, >100 μM). This clearly indicates that the cell killing activities of the complex are more specific towards cancer cells and are non-toxic to non-cancerous cells. Previous studies have shown that the non-covalently DNA binding complexes are excellent cytotoxic agents than the covalently DNA binding complexes [65,66]. Palaniandavar et al. established that copper(II) complexes, which exhibit higher DNA binding affinity and prominent DNA cleavage activity, display efficient cytotoxicity and anticancer properties [65,66]. Thus, interestingly, the quinonyl complex **1** (IC_{50}, 2.0–7.6 μM) shows cell killing activity higher than that of its benzimidazolyl analogues **2** and **3** (IC_{50}, 12.4–16.4 μM) [35] but lower than that of its pyridyl analogue, [Cu(pyrimol)Cl] **4** (IC_{50}, 3.4–3.6 μM) [16] revealing that quinonyl complex enhances the cytotoxicity. Thus, the highest cytotoxicity exhibited by **4** is consistent with the strong intercalation of the highly planar conjugated copper complex between the base pairs and its efficient DNA cleavage activity without reductant. The lowest cytotoxicity revealed by **2** and **3** is due to weak DNA binding of the complexes and they do not participate in the DNA cleavage activity. However, the enhanced cytotoxicity of **1** is attributed to the stronger binding of the complex through partial intercalative insertion of extended planar quinolyl ring between the base pairs and its higher cleavage activity with the reductant is responsible for its potency to induce cell death.

4. Conclusions

A mononuclear copper(II) complex [Cu(quamol)Cl], where H(quamol) is a N_2O tridentate ligand, has been isolated. The electronic and EPR spectral studies reveal a distorted square-planar CuN_2OCl coordination environment. The interaction of the complex with CT DNA and BSA has been investigated using different spectral techniques. Results suggest that the complex binds to DNA with a partial intercalative interaction mode, exhibits strong binding ability and effectively cleaves ϕX174 supercoiled phage DNA in the presence of ascorbic acid. Electrochemical studies on DNA-bound copper(II) complex reveals the preference of DNA to interact with Cu(II) over Cu(I) species. The copper(II) complex binds to BSA in the hydrophobic region with a moderate affinity through a static mode and induces conformational changes with the loss of α-helix stability. Interestingly, under *in vitro* conditions, the complex exhibits higher cytotoxic activity toward M19 MEL and EVSA-T and moderate activity for MCF7 cell lines. The IC_{50} value is more or less equal to that of the clinically-used cisplatin and is found to be non-toxic to normal mouse embryonic fibroblasts cells. The cytotoxicity may originate from its ability to bind to DNA to cause a conformational change in DNA and cleave it. Thus, these results provide grounds to suggest that [Cu(quamol)Cl] is a promising complex that deserves further scrutiny as an anticancer drug for treating melanoma, breast cancer and possibly other forms of cancer.

Acknowledgements

We are grateful to the DST-FIST programme of the National College (Autonomous), Tiruchirappalli. Thanks are also due to SAIF, Indian Institute of Technology Madras for recording EPR and NMR spectra. Authors thank Professor A. Ramu, School of Chemistry, Madurai Kamaraj University for CD spectral measurements.

Appendix A. Supplementary data

Supplementary data associated with this article can be found, in the online version, at https://doi.org/10.1016/j.ijbiomac.2017.10.131.

References

[1] L. Kelland, The resurgence of platinum-based cancer chemotherapy, Nat. Rev. Cancer 7 (2007) 573–584.
[2] S.Van Zutphen, J. Reedijk, Targeting platinum anti-tumour drugs: overview of strategies employed to reduce systemic toxicity, Coord. Chem. Rev. 249 (2005) 2845–2853.
[3] R.W.Y. Sun, C.M. Che, The anti-cancer properties of gold(III) compounds with dianionic porphyrin and tetradentate ligands, Coord. Chem. Rev. 253 (2009) 1682–1691.
[4] E. Wong, C.M. Giandomenico, Current status of platinum-based antitumor drugs, Chem. Rev. 99 (1999) 2451–2466.
[5] D. Chatterjee, A. Mitra, G.S. De, Ruthenium polyaminocarboxylate complexes, Platinum Met. Rev. 50 (2006) 2–12.
[6] G. Zuber, J.C. Quada, S.M. Hecht, Sequence selective cleavage of a DNA octanucleotide by chlorinated bithiazoles and bleomycins, J. Am. Chem. Soc. 120 (1998) 9368–9369.
[7] V.S. Li, D. Choi, Z. Wang, L.S. Jimenez, M.S. Tang, H. Kohn, Role of the C-10 substituent in mitomycin C-1-DNA bonding, J. Am. Chem. Soc. 118 (1996) 2326–2331.
[8] R. Palchaudhri, P.J. Hergenrother, DNA as a target for anticancer compounds: methods to determine the mode of binding and the mechanism of action, Curr. Opin. Biotechnol. 18 (2007) 497–503.
[9] G. Bischoff, S. Hoffmann, DNA-binding of drugs used in medicinal therapies, Curr. Med. Chem. 9 (2002) 321–348.
[10] J.J.R. Fraústo da Silva, R.J.P. Williams, The Biological Chemistry of the Elements – The Inorganic Chemistry of Life, Oxford University Press, Oxford, 1991.

[11] D.S. Sigman, A. Mazumder, D.M. Perrin, Chemical nucleases, Chem. Rev. 93 (1993) 2295–2316.
[12] D.K. Chand, H.J. Schneider, A. Bencini, A. Bianchi, C. Giorgi, S. Ciattini, B. Valtancoli, Affinity and nuclease activity of macrocyclic polyamines and their Cu(II) complexes, Chem. Eur. J. 6 (2000) 4001–4008.
[13] S. Dhar, D. Senapati, P.K. Das, P. Chattopadhyay, M. Nethaji, A.R. Chakravarty, Ternary copper complexes for photocleavage of DNA by red light: direct evidence for sulfur-to- copper charge transfer and d-d band involvement, J. Am. Chem. Soc. 125 (2003) 12118–12124.
[14] B.K. Santra, P.A. Reddy, G. Neelakanta, S. Mahadevan, M. Nethaji, A.R. Chakravarty, Oxidative cleavage of DNA by a dipyridoquinoxaline copper(II) complex in the presence of ascorbic acid, J. Inorg. Biochem. 89 (2002) 191–196.
[15] F.B. Tamboura, M. Gaye, A.S. Sall, A.H. Barry, T.T. Jouini, Synthesis, properties and X-ray structure for the mononuclear complex of [{(1-methyl imidazol-2-yl)methylene}-2aminoethylpyridine]-dichloro copper(II) monohydrate, Inorg. Chem. Commun. 5 (2002) 35–238.
[16] P.U. Maheswari, S. Barends, S. Ozalp-Yaman, P. de Hoog, H. Casellas, S.J. Teat, C. Massera, M. Lutz, A.L. Spek, G.P. van Wezel, B. Kozlevcar, P. Gamez, J. Reedijk, The square-planar cytotoxic [Cu(II)(pyrimol)Cl] complex acts as an efficient DNA cleaver without reductant, J. Am. Chem. Soc. 128 (2006) 710–711.
[17] C.H. Ng, K.C. Kong, S.T. Von, P. Balraj, P. Jensen, E. Thirthagiri, H. Hamada, M. Chikira, Synthesis, characterization, DNA-binding study and anticancer properties of ternary metal(II) complexes of edda and an intercalating ligand, Dalton Trans. (2008) 447–454.
[18] S. Ramakrishnan, V. Rajendiran, M. Palaniandavar, V.S. Periasamy, B.S. Srinag, H. Krishnamurthy, M.A. Akbarsha, Induction of cell death by ternary copper(II) complexes of L-tyrosine and diimines: role of coligands on DNA binding and cleavage and anticancer activity, Inorg. Chem. 48 (2009) 1309–1322.
[19] M. Peng, S. Shi, Y. Zhang, Influence of Cd^{2+}, Hg^{2+} and Pb^{2+} on (+)-catechin binding to bovine serum albumin studied by fluorescence spectroscopic methods, Spectrochim. Acta Part A: Mol. Biomol. Spectrosc. 85 (2012) 190–197.
[20] T. Peter, Serum albumin, J. Adv. Protein Chem. 37 (1985) 161–245.
[21] T. Peters, Advances in Protein Chemistry, Academic, New York, 1985.
[22] T. Chakraborty, I. Chakraborty, S.P. Moulik, S. Ghosh, Physicochemical and conformational studies on BSA-surfactant interaction in aqueous medium, Langmuir 25 (2009) 3062–3072.
[23] J.B. Chaires, Drug—DNA interactions, Curr. Opin. Struct. Biol. 8 (1998) 314–320.
[24] T. Jia, Z. Jiang, K. Wang, Z. Li, Binding and photocleavage of cationic porphyrin-phenylpiperazine hybrids to DNA, Biophys. Chem. 119 (2006) 295–302.
[25] M.R. Boyd, V.T. De Vita Jr, S.A. Rosenberg, Cancer: Principles and Practice of Oncology Update, vol. 3, Lippincott, Philadelphia, 1989, pp. 1–12.
[26] J. Marmur, A procedure for the isolation of deoxyribonucleic acid from micro-organisms, J. Mol. Biol. 3 (1961) 208–218.
[27] Y.P. Keepers, P.E. Pizao, G.J. Peters, J. van Ark-Otte, B. Winograd, H.M. Pinedo, Comparison of the sulforhodamine B protein and tetrazolium (MTT) assays for in vitro chemosensitivity testing, Eur. J. Cancer Clin. Oncol. 27 (1991) 897–900.
[28] S. Roy, K.D. Hagen, P.U. Maheswari, M. Lutz, A.L. Spek, J. Reedijk, G.P. van Wezel, Phenanthroline derivatives with improved selectivity as DNA-targeting anticancer or antimicrobial drugs, ChemMedChem 3 (2008) 1427–1434.
[29] K. Nakamoto, Infrared and Raman Spectra of Inorganic and Coordination Compounds, Wiley, New York, 1986, pp. 241–244.
[30] P. Štarha, Z. Trávníček, R. Herchel, I. Popa, P. Suchý, J. Vančo, Dinuclear copper(II) complexes containing 6-(benzylamino)purines as bridging ligands: synthesis, characterization, and in vitro and in vivo antioxidant activities, J. Inorg. Biochem. 103 (2009) 432–440.
[31] M. Vaidayanathan, R. Viswanathan, M. Palaniandavar, T. Balasubramanian, P. Prabhaharan, T.P. Muthiah, Copper(II) complexes with unusual axial phenolate coordination as structural models for the active site in galactose oxidase: X-ray crystal structures and spectral and redox properties of [Cu(bpnp)X] complexes, Inorg. Chem. 37 (1998) 6418–6427.
[32] A.B.P. Lever, Inorganic Electronic Spectroscopy, Elsevier, Amsterdam, 1984.
[33] P. Tamil Selvi, M. Murali, M. Palaniandavar, M. Köckerling, G. Henkel, X-ray crystal structure of tetrakis(1-methylcytosine)copper(II) perchlorate dihydrate: effect of 1-methyl substitution on cytosine on the spectral and redox behavior, Inorg. Chim. Acta 340 (2002) 139–146.
[34] M. Palaniandavar, I. Somasundaram, M. Lakshiminarayanan, H. Manohar, Stabilisation of unusual simultaneous binding of four cytosine nucleobases to copper(II) by a novel network of bifurcated hydrogen bonding, J. Chem. Soc. Dalton Trans. (1996) 1333–1340.
[35] C. Rajarajeswari, R. Loganathan, M. Palaniandavar, E. Suresh, A. Riyasdeen, M.A. Akbarsha, Copper(II) complexes with 2NO and 3N donor ligands: synthesis, structures and chemical nuclease and anticancer activities, Dalton Trans. 42 (2013) 8347–8363.
[36] U. Sakaguchi, A.W. Addison, Spectroscopic and redox studies of some copper(II) complexes with biomimetic donor atoms: implications for protein copper centres, J. Chem. Soc. Dalton Trans. (1979) 600–608.
[37] N. Grover, T.W. Welch, T.A. Fairley, M. Cory, H.H. Thorp, Covalent binding of aquaruthenium complexes to DNA, Inorg. Chem. 33 (1994) 3544–3548.
[38] A. Raja, V. Rajendiran, P.U. Maheswari, R. Balamurugan, C.A. Kilner, M.A. Halcrow, M. Palaniandavar, Copper(II) complexes of tridentate pyridylmethylethylenediamines: role of ligand steric hindrance on DNA binding and cleavage, J. Inorg. Biochem. 99 (2005) 1717–1732.
[39] V.I. Ivanov, L.E. Minchenkova, A.K. Schyolkina, A.I. Polytayer, Different conformations of double-stranded nucleic acid in solution as revealed by circular dichroism, Biopolymers 12 (1973) 89–110.
[40] J.G. Collins, T.P. Shields, J.K. Barton, ^{1}H NMR of $[Rh(NH_3)_4phi]^{3+}$ bound to $d(TGGCCA)_2$: classical intercalation by a nonclassical octahedral metallointercalator, J. Am. Chem. Soc. 116 (1994) 9840–9846.
[41] J.W. Chen, X.Y. Wang, Y. Chao, J.H. Zhu, Y.G. Zhu, Y.Z. Li, Q. Xu, A Trinuclear copper(II) complex of 2,4,6-tris(di-2-pyridylamine)-1,3,5-triazine shows prominent DNA cleavage activity, Inorg. Chem. 46 (2007) 3306–3312.
[42] J.R. Lakowicz, G. Webber, Quenching of fluorescence by oxygen. A probe for structural fluctuations in macromolecules, Biochemistry 12 (1973) 4161–4170.
[43] M. Lee, A.L. Rhodes, M.D. Wyatt, S. Forrow, J.A. Hartley, GC base sequence recognition by oligo(imidazolecarboxamide) and C-terminus-modified analogues of distamycin deduced from circular dichroism, proton nuclear magnetic resonance, and methidiumpropylethylenediaminetetraacetate-iron(II) footprinting studies, Biochemistry 32 (1993) 4237–4245.
[44] M. Ganeshpandian, R. Loganathan, E. Suresh, A. Riyasdeen, M.A. Akbarsha, M. Palaniandavar, New ruthenium(II) arene complexes of anthracenyl-appended diazacyclo alkanes: effect of ligand intercalation and hydrophobicity on DNA and protein binding and cleavage and cytotoxicity, Dalton Trans. 43 (2014) 1203–1219.
[45] B. Monica, B.F. Marisa, B. Franco, P. Giorgio, P. Silvana, T. Pieralberto, Cu(II) complexes with heterocyclic substituted thiosemicarbazones: the case of 5-formyluracil. Synthesis, characterization, X-ray structures, DNA interaction studies, and biological activity, Inorg. Chem. 42 (2003) 2049–2055.
[46] A.J. Bard, L.R. Faulkner, Electrochemical Methods: Fundamentals and Applications, Wiley, New York, 1980.
[47] S. Sangeetha, M. Murali, Water soluble copper(II) complex $[Cu(dipica)(CH_3COO)]\ ClO_4$: DNA binding, pH dependent DNA cleavage and cytotoxicity, Inorg. Chem. Commun. 59 (2015) 46–49.
[48] X. Zhao, R. Liu, Z. Chi, Y. Teng, P. Qin, New insights into the behavior of bovine serum albumin adsorbed onto carbon nanotubes: comprehensive spectroscopic studies, J. Phys. Chem. B 114 (2010) 5625–5631.
[49] Y. Li, W.Y. He, C.X. Xue, Z.D. Hu, X.G. Chen, F.L. Sheng, Effect of Chinese medicine alpinetin on the structure of human serum albumin, Bioorg. Med. Chem. 13 (2005) 1837–1845.
[50] A. Sulkowska, J. Równicka, B. Bojko, W. Sułkowski, Interaction of anticancer drugs with human and bovine serum albumin, J. Mol. Struct. 651 (2003) 133–140.
[51] P.D. Ross, S. Subramanian, Thermodynamics of protein association reactions: forces contributing to stability, Biochemistry 20 (1981) 3096–3102.
[52] C. Nain Lunardi, A. Claudio Tedesco, T.L. Kurth, I.M. Brinn, The complex between 9-(n- decanyl)acridone and bovine serum albumin. Part 2. What do fluorescence probes probe? Photochem. Photobiol. Sci. 2 (2003) 954–959.
[53] J.N. Miller, Recent advances in molecular luminescence analysis, Proc. Anal. Div. Chem. Soc. 16 (1979) 203–208.
[54] W. He, Y. Li, C. Xue, Z. Hu, X. Chen, F. Sheng, Effect of Chinese medicine alpinetin on the structure of human serum albumin, Bioorg. Med. Chem. 13 (2005) 1837–1845.
[55] S.M. Kelly, T.J. Jess, How to study proteins by circular dichroism, Biochem. Biophys. Acta 1751 (2005) 119–139.
[56] Y. Jin, J.A. Cowan, DNA cleavage by copper-ATCUN complexes. Factors influencing cleavage mechanism and linearization of dsDNA, J. Am. Chem. Soc. 127 (2005) 8408–8415.
[57] O.I. Aruoma, B. Halliwell, M. Dizdaroglu, Iron ion-dependent radical-generating modification of bases in DNA by the superoxide system hypoxanthine/xanthine oxidases, J. Biol. Chem. 264 (1989) 13024–13028.
[58] K. Yamamoto, S. Kawanishi, Hydroxyl free radical is not the main active species in site- specific DNA damage induced by copper (II) ion and hydrogen peroxide, J. Biol. Chem. 264 (1989) 15435–15440.
[59] R. Nilsson, P.B. Merkel, D.R. Keams, Unambiguous evidence for the participation of singlet oxygen (1) in photodynamic oxidation of amino acids, Photochem. Photobiol. 16 (1972) 117–124.
[60] M.D. Kuwabara, C. Yoon, T. Goyne, T. Thederahn, D.S. Sigman, Nuclease activity of 1,10-phenanthroline-copper ion: reaction with CGCGAATTCGCG and its complexes with netropsin and EcoRI, Biochemistry 25 (1986) 7401–7408.
[61] A. Amine, Z. Atmani, A. El Hallaoui, M. Giorgi, M. Pierrotc, M. Réglierc, $Copper(II)/H_2O_2$-mediated DNA cleavage: involvement of a copper(III) species in H-atom abstraction of deoxyribose units, Bioorg. Med. Chem. Lett. 12 (2002) 57–60.
[62] M.M. Meijler, O. Zlelnko, D.S. Sigman, Chemical mechanism of DNA scission by (1,10-phenanthroline)copper. Carbonyl oxygen of 5-methylenefuranone is derived from water, J. Am. Chem. Soc. 119 (1997) 1135–1136.
[63] D.S. Sigman, M.D. Kuwabara, C.B. Chen, T.W. Bruice, Nuclease activity of 1,10-phenanthroline-copper in study of protein-DNA interaction, Methods Enzymol. 208 (1991) 414–433.
[64] L. Ingrassia, P. Nshimyumukiza, J. Dewelle, F. Lefranc, L. Wlodarczak, S. Thomas, G. Dielie, C. Chiron, C. Zedde, P. Tisnes, R. van Soest, J.C. Braekman, F. Darro, R.A. Kiss, Lactosylated steroid contributes in vivo therapeutic benefits in experimental models of mouse lymphoma and human glioblastoma, J. Med. Chem. 49 (2006) 1800–1807.

Please cite this article in press as: S. Sangeetha, M. Murali, Int. J. Biol. Macromol. (2017), https://doi.org/10.1016/j.ijbiomac.2017.10.131

[65] R. Loganathan, S. Ramakrushnan, E. Suresh, A. Riyasdeen, M.A. Akbarsha, M. Palaniandavar, Mixed ligand copper(II) complexes of N,N-bis(benzimidazol-2-ylmethyl)- amine (BBA) with diimine co-Ligands: efficient chemical nuclease and protease activities and cytotoxicity, Inorg. Chem. 51 (2012) 5512–5532.

[66] M. Ganesh Pandian, R. Loganathan, S. Ramakrishnan, E. Suresh, A. Riyasdeen, M.A. Akbarsha, M. Palaniandavar, Interaction of mixed ligand copper(II) complexes with CT DNA and BSA: effect of primary ligand hydrophobicity on DNA and protein binding and cleavage and anticancer activities, Polyhedron 52 (2013) 924–938.

Please cite this article in press as: S. Sangeetha, M. Murali, Int. J. Biol. Macromol. (2017), https://doi.org/10.1016/j.ijbiomac.2017.10.131